

Cupid is Doomed: An Analysis of the Stability of the Inner Uranian Satellites

Robert S. French<sup>a,\*</sup> and Mark R. Showalter<sup>b</sup>

<sup>a</sup>SETI Institute, 189 Bernardo Ave., Mountain View, California 94043, United States;  
rfrench@seti.org

<sup>b</sup>SETI Institute, 189 Bernardo Ave., Mountain View, California 94043, United States;  
mshowalter@seti.org

\* Corresponding Author:

Robert S. French  
SETI Institute  
189 Bernardo Ave.  
Mountain View, CA 94043 United States  
Phone: 1+408-802-2635  
Fax: 1+866-688-4691  
E-mail address: rfrench@seti.org

## ABSTRACT

We have explored the stability of the inner Uranian satellites using simulations based on the most recent observational data. We find that, across a wide range of mass assumptions, the system is chaotic, resulting in the eventual crossing of orbits. Cupid and Belinda are usually the first satellites to cross orbits, and they do so on a time scale of  $10^3$ – $10^7$  years. Cressida and Desdemona are generally the next pair to cross, on a time scale of  $10^5$ – $10^7$  years. We show that the crossing times are highly sensitive to initial conditions and that Cupid's instability is related to its resonant interactions with Belinda. We also show that a previously discovered power law, with which the orbit crossing time can be predicted using multiple, shorter simulations with higher mass assumptions, is valid across a wide range of masses. We generalize the power law to handle two unstable orbital pairs with overlapping lifetimes, and show it can be used to further extend the range of mass assumptions in a computationally efficient manner.

**Key Words:** Uranus, satellites; Satellites, dynamics; Resonances, orbital

## 1. INTRODUCTION

Uranus has the most densely-packed system of low-mass satellites close to the planet (semi-major axes  $a = 59,166\text{--}97,736$  km or 2.3–3.8 Uranian radii) in the solar system. Ten of these satellites were discovered by Voyager 2 (Smith et al., 1986). Perdita was discovered later in archival Voyager 2 imagery (Karkoschka, 2001a), and Cupid and Mab were discovered using the Hubble Space Telescope (HST) (Showalter and Lissauer, 2006). In addition to these inner satellites, Uranus has five large “classical” satellites ( $a = 129,848\text{--}583,520$  km) as well as nine very distant “irregular” satellites ( $a = 4.2\times 10^6\text{--}2.1\times 10^7$  km).

Multiple observations of the inner satellites provided by Voyager 2 (Smith et al., 1986), simultaneous analysis of data from HST and Voyager 2 (Owen and Synnott, 1987; Jacobson, 1998), and 15 years of HST observations (Showalter et al., 2008; 2010) have shown that the orbits of the inner satellites are variable over periods shorter than two decades. If the system is chaotic, the orbits of two or more satellites may eventually cross. Such a crossing is likely to lead to close approaches and possibly an eventual collision of the two satellites because of the unequal precession of the orbits as well as continued interactions between the various satellites (Mikkola and Innanen, 1995).

Several prior studies of the orbital stability of the inner satellites have been conducted. Duncan and Lissauer (1997, henceforth DL97) studied the orbital dynamics of a subset of eight of the inner satellites along with the five classical satellites using the SWIFT Regularized Mixed Variable Symplectic simulator (Levison and Duncan, 1994). They ran simulations until two satellites crossed orbits or until a preset time limit was exceeded. Initial orbital state vectors for the inner satellites were taken from Voyager 2 images (Owen and Synnott, 1987), and those for the classical satellites were taken from previously unpublished measurements. Because the dynamical masses of the inner satellites are unknown, DL97 used mass estimates by Lissauer (1995), which are based on estimated radii from unresolved images (Thomas et al., 1989) and the assumption that the densities are the same as that of Miranda,  $\rho = 1.2$  g/cm<sup>3</sup> (Jacobson et al., 1992).

Due to the time required to execute their simulations, DL97 were unable to explore a wide range of realistic mass estimates. Instead, they assumed a single set of mass estimates and then introduced a *mass scaling factor*,  $m_f$ , that was uniformly applied to all satellites. Comparing the time to first orbit crossing,  $t_c$ , with  $m_f$ , they found that orbit crossing time generally decreased with increasing mass, presumably due to the stronger mutual perturbations. The results were well-described by a power law of the form  $t_c = \beta m_f^\alpha$ . Thus, by running a large number of simulations with  $m_f > 1$ , DL97 could find  $\alpha$  and  $\beta$  and thus extrapolate to  $t_c(m_f=1)$ . They found that the five classical satellites, by themselves, were stable over a period much longer than the age of the solar system ( $\sim 2.5\times 10^{17}$  years), while the inner satellites were stable over a much shorter period ( $\sim 4\text{--}100$  million years), with either Cressida and Desdemona or Desdemona and Juliet crossing orbits within this time. When the oblateness of Uranus was taken into account (an assumption used throughout our analysis), the presence of the classical satellites did not substantially affect the orbit-crossing times, presumably because the resulting orbital precession disrupted any secular resonances that would otherwise form.

Meyer and Lissauer (2005) used the Mercury hybrid symplectic integrator (Chambers, 1999) to simulate the same 13 satellites used by DL97. They explored a range of possible masses by assuming densities from 0.1–30 g/cm<sup>3</sup> and replicated the fundamental results of DL97 by showing that the inner satellites generally experienced collisions in less than  $3\times 10^6$  years, with

lower densities corresponding to longer times between collisions. By assuming perfectly inelastic collisions, they also continued the simulations past the first collision to explore further system development and modeled the effects of tidal damping on eccentricities. The fact that the simulations of Meyer and Lissauer (2005) experienced collisions over time periods similar to the orbit crossings found by DL97 adds weight to the argument that a collision will shortly follow the crossing of two orbits.

Dawson et al. (2009; 2010; 2011) explored the short-term evolution of the orbits of the inner Uranian satellites by analyzing the effects of overlapping resonances and also by computing the Lyapunov characteristic exponent for each satellite. They found that the orbital evolution was very sensitive to the assumed masses and attributed this sensitivity to the dependence of the widths of the overlapping resonances to the masses. They also found that the Lyapunov time increased with decreased mass, but numerical artifacts prevented them from determining if the system ever became stable with sufficiently small masses.

In this study, we take advantage of the increase in computational speed since 1997 and expand upon the results of DL97. We first examine the orbital stability of the Uranian satellites by direct integration without using the power law. We explore a range of mass estimates and densities for the inner satellites, include the inner satellites omitted by DL97 (Cordelia and Ophelia), and add the three more recently discovered satellites Cupid, Perdita, and Mab. We also investigate the effect of including the classical satellites, as well as removing individual satellites from the model, and examine the resonant interactions between various satellite pairs. However, as the power law does have its uses for low-mass systems when simulation times become prohibitive, we also test the validity of the power law with a wide range of mass factors and extend the power law to the case where there are two independent unstable systems with overlapping orbit crossing times. Finally, we investigate the possible future evolution of the satellite system.

The paper is organized as follows. In Section 2 we discuss the simulation methodology, including the choice of simulator and computation environment, the selection of satellite masses and orbital parameters, and the analysis of the numerical stability of the simulation. In Section 3 we analyze the stability of the orbits under the various mass assumptions without using the power law, and we examine the effect of including the classical satellites in the model as well as the effect of removing individual inner satellites. In Section 4 we reproduce and expand upon the results of DL97 to verify the applicability of the power law over a larger range of mass factors, extend the power law to handle the case of two overlapping unstable satellite systems, and analyze our new models using the power law. In Section 5 we examine other indicators of orbital chaos and discuss the long-term evolution of the satellite system. Finally, in Section 6 we discuss the implications of our results and present concluding remarks.

## 2. METHODOLOGY

### 2.1. Simulator and Environment

All simulations were performed using the SWIFT<sup>1</sup> simulator and the RMVS3 Regularized Mixed Variable Symplectic integrator (Levison and Duncan, 1994), which is based on the symplectic mapping method of Wisdom and Holman (1991). We applied minor modifications to

---

<sup>1</sup> SWIFT is available at <http://www.boulder.swri.edu/~hal/swift.html>.

the SWIFT driver to check for orbit crossings and to change the format of the output file, but the core algorithm was unchanged.

We define the crossing time,  $t_c$ , as the time when the apoapsis of any one satellite becomes larger than the periapsis of the next satellite out from Uranus. For convenience, we will often refer to  $\log t_c$ , the base 10 logarithm with  $t_c$  measured in seconds; to convert to units of years, subtract 7.5. We used the traditional osculating element definitions for the eccentricity and semi-major axis to compute the periapses and apoapses. These are known to contain errors in the presence of an oblate central body, but are simple and fast to compute. Crossing times using osculating elements were compared across a wide range of simulations to crossing times computed using the geometric orbital elements of Borderies-Rappaport and Longaretti (1994), and in 99% of the cases the crossing times did not differ. In the remaining small number of cases, the difference was minor, and we do not expect the use of osculating elements to compute crossing times to materially affect our analysis.

The majority of the runs, as well as the computationally-intensive orbital fits, were performed using the 1,160-processor supercomputer at the Centre for Astrophysics and Supercomputing at the Swinburne University of Technology. Additional simulations were performed on various desktop PCs running the 64-bit version of Windows 7. In all cases, SWIFT was compiled with the GNU 3.4 32-bit FORTRAN 77 compiler. A direct comparison of simulation results from the various systems showed no difference.

As the numerical stability of the SWIFT simulator has already been well-established in previous studies (e.g., Levison and Duncan, 1994; DL97), we did not repeat this work. However, to determine the appropriate simulation parameters, we characterized the sensitivity of orbit crossing time to integration step size. As expected, we found no systematic dependence as long as the step size was kept sufficiently small. After balancing the tradeoffs between precision and integration speed, we settled on a step size of  $1/20^{\text{th}}$  the period of the innermost satellite, the same step size used by DL97 for the majority of their simulations. This resulted in a step size of 1,887.381 sec when simulating the set of satellites used by DL97 (with Bianca innermost) and 1,447.347 sec when simulating our more complete set (with Cordelia innermost).

## 2.2. Satellites and mass estimates

We used two different sets of satellites, masses, and physical parameters in this study. The first set included those used by DL97 as part of their “8J” and “13J” models, which we will refer to as DL97(8J) and DL97(13J), respectively. The DL97(8J) model used the satellites in the “Portia group” (Bianca, Cressida, Desdemona, Juliet, Portia, Rosalind, Belinda, and Puck). The DL97(13J) model added the five classical satellites Miranda, Ariel, Umbriel, Titania, and Oberon. The assumed masses can be found in Table 1 and the initial state vectors can be found in DL97. DL97 assumed a radius for Uranus of  $R_U = 26,200$  km and quadrupole and octopole gravitational moments for Uranus of  $J_2 = 3.34343 \times 10^{-3}$  and  $J_4 = -2.885 \times 10^{-5}$  from French et al. (1991). Since DL97 did not publish their assumptions for the  $GM$  of Uranus, we assumed a value of  $5793965.663939 \text{ km}^3 \text{ s}^{-2}$  in our simulations.<sup>2,3</sup>

---

<sup>2</sup> From the ura083.bsp SPICE kernel, available at [http://naif.jpl.nasa.gov/pub/naif/generic\\_kernels/spk/satellites/ura083.bsp](http://naif.jpl.nasa.gov/pub/naif/generic_kernels/spk/satellites/ura083.bsp).

<sup>3</sup> Throughout this paper, we present full 16-digit machine precision for all physical quantities that are used during simulation. This should not be construed to represent the level of precision actually available in the measurements, which is usually substantially less. Instead, because of the sensitivity of the chaotic systems to small changes in input parameters, we provide the full precision so that our results may be reproduced.

We produced a second set of satellites, masses, and physical parameters based on updated data. We included Cordelia and Ophelia, and we also added the three inner satellites discovered since 1997, Cupid, Perdita, and Mab. No dynamical mass estimates are available for the 13 inner satellites, and masses computed based on volume and density are subject to errors in observed radius as well as unknown density. Measurements of radii are particularly error-prone because the inner satellites have very low ( $< 0.07$ ) and poorly measured albedos (Smith et al., 1986; Karkoschka, 2001b). As an extreme example, if Mab has the albedo of the next innermost satellite, Puck, it has a radius of 12 km, while if it has the albedo of the next outermost satellite, Miranda, it has a radius of 6 km, resulting in a factor of eight uncertainty in volume (Showalter and Lissauer, 2006). However, resolved Voyager images have permitted the determination of the albedo of many of the satellites with reasonable accuracy, and this has permitted the calculation of updated size estimates (Karkoschka, 2001a).

We have assumed that all of the inner satellites except Cupid, Perdita, and Mab have the radii and  $1 \sigma$  errors found by Karkoschka (2001a). For the remaining three satellites, we have used the radii found by Showalter and Lissauer (2006) and assumed a 20% uncertainty in albedo and a 20% uncertainty in disk-integrated photometry. This yields a 40% error in area and thus a  $\sim 20\%$   $1 \sigma$  error in radius. In all cases, we have assumed an initial density of  $1 \text{ g/cm}^3$ , which is less than the density of  $1.2 \text{ g/cm}^3$  assumed by DL97, and computed the mass accordingly (Table 1). We call this set of assumptions I(baseline), where the “I” indicates the use of the inner 13 satellites and the “baseline” indicates the use of the baseline radius assumption. Despite the lower density assumption, the increased radii nevertheless result in baseline masses that are, on average,  $\sim 55\%$  larger than those assumed by DL97, and we expect these larger masses to cause greater perturbations and thus shorter orbit crossing times.

To account for uncertainties in radius, we created additional sets of mass assumptions. For each of the 13 satellites, we assumed that its radius was  $1 \sigma$  below, and also  $1 \sigma$  above, the baseline estimate, while the rest of the satellites were held at their baseline radius. This resulted in an additional 26 mass combinations labeled I(*sat*-) and I(*sat*+), where *sat* is one of the 13 Uranian satellites that has had its radius perturbed (as indicated in Table 1), and the - or + indicates the direction in which it was changed. In addition, several models were created to account for the uncertainty in density. In these cases, the model name has an additional parameter indicated by “/density”, such as I(baseline/1.5), where density is in units of  $\text{g/cm}^3$ . If no density is specified, a density of  $1 \text{ g/cm}^3$  is assumed.

We have also created models that include the five classical satellites. The model containing only these five satellites, with none of the inner satellites, is called O(). The models containing all 18 satellites are called IO(baseline) and C(baseline), where the masses are the same but the initial state vectors are determined differently as described in the following section. The masses of the classical satellites, which are known dynamically, are never modified.

For our new models, we assume a radius for Uranus of  $R_U = 26,200 \text{ km}$ , quadrupole and octopole gravitational moments for Uranus of  $J_2 = 3.344247802666718 \times 10^{-3}$  and  $J_4 = -2.772599495619087 \times 10^{-5}$ , and a  $GM$  for Uranus of  $5793965.663939 \text{ km}^3\text{s}^{-2}$  (all from the SPICE “ura083.bsp” kernel).

### 2.3. Initial orbital state vectors

The orbits of the inner satellites are constrained by a series of unevenly spaced observations made over the past 24 years, first by Voyager 2 and more recently by the Hubble Space

Telescope. We wish our simulations to agree as closely as possible with these observations over this time period, and thus must find a set of initial state vectors (three-dimensional position and velocity) for our simulations that result in the best positional matches. All relevant astrometric data has been collected by the Navigation and Ancillary Information Facility (NAIF) at NASA's Jet Propulsion Laboratory and used to create a set of standard orbital models that are published in the form of data kernels for the SPICE information system.<sup>4</sup> The orbits for the inner satellites are modeled as simple precessing ellipses because perturbations are expected to be small over such a short time, and because insufficient observations are available for more elaborate modeling (Jacobson, 1998). The model orbits for the classical satellites are provided from numerical integration orbital fits of available astrometric data. We used these models to provide observational constraints for our orbital fits, with "ura091.bsp"<sup>5</sup> containing the models of the inner satellites and "ura083.bsp" containing the models of the classical satellites.

The SPICE library provides the ability to calculate the state vector of each satellite from its model at any time from January 3, 1910 to January 4, 2050. However, because of the highly variable mutual perturbations of the satellites, a simulation initialized from state vectors derived from these models at one time and run until a later time will not produce the same sequence of satellite positions as would be retrieved from the SPICE models over that time interval. In addition, the amount that the initial state vectors must be modified to make the simulation results agree as closely as possible with the models over the valid time will depend heavily on the masses of the satellites, which in turn govern the extent of the perturbations. Thus any change in the masses requires a new computation of the initial state vectors.

To compute the initial state vectors that result in the best agreement between simulation and model over a reasonable time period, we performed an iterative orbital fit over the period January 1, 1986 to January 1, 2010, the approximate range of available observations. The fit consisted of a four-pass Powell optimization (Powell, 1964) over the six-dimensional vector of orbital elements for each satellite, which was sufficient to produce state vector components accurate to less than 1 mm or 1 mm/sec. The orbital elements were initialized for 00:00:00 UTC on January 1, 1986 based on conversion from the state vectors provided by the SPICE library. We chose to use the geometric orbital elements of Borderies-Rappaport and Longaretti (1994), as implemented in closed-form solution by Renner and Sicardy (2006), during the fit procedure because they are not subject to the short-term oscillations present in the osculating elements caused by Uranus' oblateness.

The optimization attempted to minimize the root-mean-square (RMS) residual between the positions produced by a SWIFT simulation and the positions produced by the models contained in the SPICE kernels. Optimization was initially performed over 1.5 days, and the time period was progressively increased to cover the entire 24-year period after seven passes. To fully optimize the state vectors for 13 satellites would require a Powell-style optimization over a 78-dimensional space (13 state vectors times six parameters per state vector). Such an optimization is computationally impractical. Thus, for each time span, each satellite was optimized separately, starting from the outermost and proceeding inwards, while the initial state vectors of the other satellites were held constant. The outer-to-inner optimization direction was chosen because the more massive outer satellites are more likely to perturb the less massive inner satellites than the reverse, and thus the initial state vectors of the inner satellites depend more strongly on the orbital solution chosen for the outer satellites.

---

<sup>4</sup> For more information on SPICE, see <http://naif.jpl.nasa.gov/naif/toolkit.html>.

<sup>5</sup> Available at [http://naif.jpl.nasa.gov/pub/naif/generic\\_kernels/spk/satellites/ura091.bsp](http://naif.jpl.nasa.gov/pub/naif/generic_kernels/spk/satellites/ura091.bsp).

Resulting orbital fits were on the order of  $10\text{--}10^5$  km RMS over the 24-year simulation period. The larger residuals were present for those satellites that had highly sensitive interactions with their neighbors. Perdita is located at the 43:44 outer Lindblad resonance of Belinda, and, while the mean perturbation caused by this resonance is modeled in the SPICE kernel, the short-term perturbations are not, resulting in an unusually large residual for Perdita. Mab is also known to show large, unexplained perturbations, including a 100-km longitudinal shift over a six-day period (Showalter and Lissauer, 2006), and these unmodeled effects cause larger residuals as well.

For the IO(baseline) and C(baseline) models, a simultaneous orbital fit was required for all 18 satellites. DL97 found that, in the presence of a  $J_2/J_4$  oblateness for Uranus, the five classical satellites did not substantially affect the orbital evolution of the inner satellites. To test this result, we optimized the orbital parameters of the I(baseline) model, which consists of only the inner satellites, and the O() model, which consists of only the classical satellites, separately. We then generated a combined model, C(baseline), containing all 18 satellites using the masses and initial state vectors from the union of the I(baseline) and O() models. We simulated the C(baseline) model for 24 years, comparing the simulated satellite positions with the SPICE-derived models. If the inner and outer satellite groups do not interact at all, the residuals of the C(baseline) model would be the same as the combined residuals of I(baseline) and O(). However, this is not the case. The presence of the inner satellites has only a small effect on the outer satellites, as would be expected, but the presence of the outer satellites has a noticeable effect on the inner satellites. The implications of the presence of the outer satellites will be discussed more in Section 3.1.

Because of the effect of the classical satellites on the inner satellites, it was necessary to perform a complete orbital fit of all 18 satellites, and the result is the IO(baseline) model. The IO(baseline) model has smaller residuals for the inner satellites than the C(baseline) model, while the reverse is true for the classical satellites. As a result, we include both models in our analysis below. We expect that a more thorough orbital fit procedure would provide an overall model superior to both IO(baseline) and C(baseline), but such a procedure was computationally impractical for this study.

### 3. STABILITY OF THE INNER SATELLITES

#### 3.1. Predictions of instability

Gladman (1993) found that a system with a central body and two close planets on circular orbits will be Hill stable (disallow close approaches) as long as the initial orbital separation of the two planets,  $\Delta = a_2 - a_1$ , is greater than  $2.4(\mu_1 + \mu_2)^{1/3}$ , where  $\mu_1$  and  $\mu_2$  are the mass ratios of the two planets to the central body. Chambers et al. (1996) expanded this result to multi-planet systems and found that, across a wide range of assumptions, a system is always unstable as long as the initial orbital separations,  $\Delta$ , now measured in units of the mutual Hill radii,  $R_H = [(m_1 + m_2) / 3M]^{1/3} [(a_1 + a_2) / 2]$ , are less than 10, while systems with  $\Delta \geq 10$  are decreasingly likely to be unstable.

We used the mass assumptions in our I(baseline) model to compute  $\Delta$  for each pair of adjacent satellites and found that the two closest separations were Cupid–Belinda ( $\Delta=10.12$ ) and Cressida–Desdemona ( $\Delta=11.78$ ). Additional close separations were provided by

Belinda–Perdita ( $\Delta=13.37$ ), Juliet–Portia ( $\Delta=13.38$ ) and Desdemona–Juliet ( $\Delta=18.39$ ). All other pairings had  $\Delta>30$ . Thus we expect that the Cupid–Belinda–Perdita and Cressida–Desdemona–Juliet–Portia systems are particularly unstable.

### 3.2. Simulation results

We can analyze the stability of the inner satellites by looking at the orbit crossing times found from direct integration. We have found this value for 32 inner satellite models (Table 2). For the models that assume a density of  $1.0 \text{ g/cm}^3$ , Cupid and Belinda are almost always the first to cross, with  $\log t_c = 11.6$  to  $13.2$  ( $1.3 \times 10^4$ – $5.0 \times 10^5$  years). Allowing a wider range of densities ( $\rho = 0.5$ – $3.0$ ) expands the range to  $10.6$  to  $13.7$  ( $1.3 \times 10^3$ – $1.6 \times 10^6$  years). As an example of orbital evolution, the apoapse and periapse of Cupid and Belinda using the I(baseline) model are shown until orbit crossing in Fig. 1.

This first crossing of Cupid and Belinda is in contrast to the results of DL97, where Cressida and Desdemona, or Desdemona and Juliet, were the first satellites to cross. As Cupid was not yet discovered at the time of DL97 and thus not included in their models, a reasonable explanation is that the Cupid–Belinda system is more unstable than the Cressida–Desdemona–Juliet system, resulting in the earlier orbit crossing of Cupid and Belinda effectively hiding a later crossing of Cressida and Desdemona. To verify this result, we conducted simulations with either Cupid or Belinda removed. The orbital fits were not recomputed and the initial state vectors from the I(baseline) model were used. The results are shown in Table 3. In these simulations, Cressida and Desdemona are the first satellites to cross, with crossing times approximately an order of magnitude longer than those found when Cupid and Belinda are present. Although DL97 was not able to find the crossing time for many of their models with direct integration, the predicted log crossing times for Cressida and Desdemona from application of the power law ranged from  $12.5$  to  $15.7$  ( $t_{c,pred} = 1.0 \times 10^5$ – $1.6 \times 10^8$  years). Their most realistic models, DL97(8J) and DL97(13J), both had predicted log crossing times of  $14.1$  ( $t_{c,pred} = 4 \times 10^6$  years). This is in comparison to log crossing times of  $13.5$  and  $13.7$  ( $1.0 \times 10^6$ – $1.6 \times 10^6$  years) in our simulations. The shorter crossing times can be accounted for by our new mass assumptions, which are  $\sim 55\%$  higher than those used by DL97.

We also explored the effect of removing each of the other inner satellites on the crossing time (Table 3). In general, the removal of a single satellite does not dramatically change the time of first orbit crossing, and Cupid and Belinda remain the first pair of satellites to cross. However, when Perdita, a very low mass satellite not present in the DL97 models, is removed, Cressida and Desdemona are once again the first satellites to cross, even though Cupid and Belinda are still present in the system, implying that the presence of Perdita destabilizes the Cupid–Belinda system. The effect of Perdita will be discussed further in Section 4.4.

Finally, we can also investigate the influence of the five classical satellites on orbit crossing time. DL97 found that the addition of these satellites did not significantly change their results as long as Uranus was assumed to be oblate (an assumption we make throughout this paper). In fact, their predicted log orbit crossing times were the same for their DL97(8J) and DL97(13J) models. To verify that the classical satellites continue to be unimportant in our new models, we analyzed the C(baseline) and IO(baseline) models (see Table 2). The result, log crossing times of  $12.9$  and  $13.1$  ( $2.5 \times 10^5$  and  $4.0 \times 10^5$  years), respectively, are close to the log crossing time of the I(baseline) model,  $12.5$ , and are comfortably within the range of  $11.6$ – $13.2$  ( $1.3 \times 10^4$ – $5.0 \times 10^5$  years) for all I(*sat* $\pm$ ) models. Thus it appears that the presence of the classical satellites

does not significantly change the chaotic behavior of the inner satellites, even though there is evidently some effect on the orbits, and we will ignore the classical satellites for the rest of this paper.

Although we predict that the Cupid–Belinda–Perdita and Cressida–Desdemona–Juliet–Portia subsets will be unstable in isolation, our simulations so far were performed with the full complement of inner satellites present. Examining the instability of these two groups of satellites in isolation permits us to determine what effect, if any, the remaining satellites have on their stability. However, it is worth noting that Juliet and Portia, despite their predicted instability, almost never cross in our simulations. The reason for this is unclear, although it is probably related to their near-resonant interaction discussed in Section 3.3, but as a result of this observation we will remove Portia from our isolation studies.

A simulation containing only Cupid, Belinda, and Perdita, with a new orbital fit, resulted in a log crossing time of 14.1 ( $\sim 3.8 \times 10^6$  years). While this is noticeably longer than any of our 13-satellite models, most of which have Cupid and Belinda crossing first, it is nevertheless clear that the Cupid–Belinda–Perdita system is unstable on astronomically short timescales even in isolation.

Likewise, a simulation containing only Cressida, Desdemona, and Juliet, with a new orbital fit, resulted in a log crossing time of 14.7 ( $\sim 1.6 \times 10^7$  years). This is noticeably longer than the log crossing times of any of our 13 satellite models, and in particular is longer than the log crossing times of 13.5–13.7 from the I(baseline) model with Cupid, Belinda, or Perdita deleted, the most similar of our models that result in a crossing of Cressida and Desdemona. Like the Cupid–Belinda–Perdita system, the Cressida–Desdemona–Juliet system is apparently unstable on its own, although on a much longer timescale. In both cases, the addition of other satellites decreases the overall stability and thus decreases the crossing time.

### *3.3. Sensitivity to initial conditions*

To explore the accuracy of our crossing times and the nature of the chaos, it is worthwhile to analyze the sensitivity of the results to small perturbations in initial conditions. To do this, we started with the I(baseline) model as a reference. This model has a log  $t_c$  of 12.5, with Cupid and Belinda crossing first. We then perturbed the initial conditions by moving, alone or in combination, the X, Y, and Z components of the initial state vector by  $-2$ ,  $-1$ ,  $0$ ,  $+1$ , and  $+2$  mm, resulting in 124 additional models. The result was a dramatic spread in crossing times, with a minimum of  $\log t_c = 11.7$  and a maximum of  $\log t_c = 13.4$ , a factor of  $\sim 50$ . The crossing times were approximately normally distributed around a mean of 12.5 with a standard deviation of 0.4. There was no correlation between the crossing times and the change made in the X, Y, or Z axes. In addition to the spread in crossing times, some simulations had different pairs of satellites (Rosalind and Cupid, or Belinda and Perdita) crossing first as well.

We further analyzed the sensitivity to initial conditions by taking the I(baseline) model and perturbing the mass of Cupid by  $-6.2 \times 10^8$  g to  $+6.2 \times 10^8$  g in increments of  $10^7$  g (a change of approximately one part in  $10^{11}$ ). Again the resulting crossing times showed a wide spread (a factor of  $\sim 130$ ) with no obvious correlation to mass, as well as a variety of crossing satellites, with the same mean and standard deviation as the position perturbation.

There is little doubt that the simulations are extremely sensitive to initial conditions, and there is no reason to believe that the precise conditions we have chosen result in representative crossing times. Thus all individual crossing times discussed in this paper must be considered to

be only one sample of a set of possible crossing times that span approximately two orders of magnitude.

### 3.4. Resonant interactions

Much of the orbital instability of the Uranian satellites can be attributed to resonant interactions. Belinda and Perdita are the most well-known example of interacting satellites, with Perdita located at Belinda's 43:44 outer Lindblad resonance (OLR). This interaction is known to cause libration in the orbit of Perdita (Showalter and Lissauer, 2006). Other resonant relationships are not as exact, but nevertheless have a clear effect on orbital evolution.

One measure of satellite interaction is the statistical correlation of the semi-major axes, a proxy for orbital energy. We generated a series of correlations using a sliding time window for each pair of satellites in the I(baseline) model and then computed the mean and standard deviation ( $\sigma$ ) of the resulting correlations. A pair of satellites that has no interaction would have a mean and standard deviation of zero, while a pair that is perfectly anticorrelated would have a mean of  $-1$  and a standard deviation of zero. A non-zero standard deviation implies that the correlation changes during the simulation, perhaps as a result of a satellite approaching and then retreating from a resonance.

In each case where we found a mean significantly different from zero, the pair of satellites was also related by a resonance. Bianca and Cressida have a mean correlation of  $-0.14$  and  $\sigma$  of  $0.24$ , with Bianca  $4.0$  km from the 16:15 inner Lindblad resonance (ILR) of Cressida. Nearby first-order resonances are spaced  $\sim 160$  km apart. Cressida and Desdemona are strongly anticorrelated, with a mean of  $-0.93$  and  $\sigma$  of  $0.05$ . Cressida is located  $0.9$  km from the 47:46 ILR of Desdemona, with first-order resonances spaced  $\sim 19$  km.

Juliet and Portia have the strongest consistent anticorrelation, with a mean of  $-0.95$  and  $\sigma$  of  $0.05$ . In this case, a second-order resonance is important, with Juliet  $1.8$  km from the 51:49 ILR of Portia. Nearby second-order resonances are spaced  $34.5$  km apart. This resonance is particularly interesting because, in our simulations, Juliet and Portia almost never cross orbits. Visual inspection of the orbital elements shows that whenever Juliet approaches the 51:49 ILR of Portia, it is repelled. This prevents Juliet and Portia from getting close enough to cross orbits.

As previously discussed, Belinda and Perdita interact through Belinda's 43:44 outer Lindblad resonance. They have a mean correlation of  $-0.63$  with a  $\sigma$  of  $0.33$ . Belinda and Puck have a mean correlation of  $-0.26$  and  $\sigma$  of  $0.14$ . Puck is  $10.1$  km from the 9:11 OLR of Belinda, with second-order resonances separated by  $\sim 925$  km.

Perhaps the most interesting resonant interaction is found between Cupid and Belinda. These satellites have a mean correlation of  $-0.36$  with a  $\sigma$  of  $0.26$ . Although the exact position of Cupid is sufficiently uncertain (Showalter and Lissauer, 2006) that placing its current position precisely in a resonance of Belinda is unlikely to be accurate, it is nevertheless enlightening to observe the orbital interaction of these satellites over time. For example, we can explore the relationship between Cupid and Belinda both before and after the onset of significant instability seen in Fig. 1. Fig. 2 shows the semi-major axis of Cupid plotted against the first- and second-order ILRs of Belinda. It is clear that Cupid tends to maintain a stable orbit at one of Belinda's ILRs, but it is occasionally kicked out of a resonance and settles into a different resonance. During the period when Cupid is moving between resonances, the semi-major axes of Cupid and Belinda become highly anti-correlated as they exchange angular momentum. However, due to

the much larger mass of Belinda, its orbit is mostly unaffected while Cupid undergoes major orbital changes.

Starting at approximately  $3.28 \times 10^{12}$  sec in this simulation, the semi-major axes of Cupid and Belinda once again become perfectly anti-correlated, and remain so until the orbit crossing occurs. Fig. 3 shows the semi-major axis of Cupid plotted against the ILRs of Belinda during this time. Cupid rapidly hops between a wide variety of first- and second-order resonances, with occasional brief periods of stability. It is clear that this interaction between Cupid and Belinda is the primary cause of Cupid's instability and their eventual orbital crossing.

## 4. THE POWER LAW

### 4.1. Introduction

DL97 found that the time of orbit crossing,  $t_c$ , could be predicted by running many simulations with the satellite masses increased by mass factors,  $m_f$ , and fitting the results to a power law of the form  $t_c(m_f) = \beta m_f^\alpha$ . The time of orbit crossing is then easy to find, because when  $m_f = 1$ ,  $t_c = \beta$ . DL97 relied heavily on the power law to make their prediction that the Uranian satellite system was unstable on the time span of 4–100 million years. However, due to computational limitations, they were only able to verify the operation of the power law for a small subset of their models. It is thus reasonable for us to ask whether the power law is truly applicable for their models and whether it is applicable to our new models as well. Of the nine models analyzed by DL97, only two were able to fully demonstrate the power law by including a simulation at  $m_f = 1$ . Both of these models, DL97(8H) and DL97(13H), did not include the Uranian  $J_2/J_4$  terms and also did not adjust the initial state vectors to account for the now-inaccurate orbital elements, making the results less relevant to the current study. The DL97(8C) model was able to get close to  $m_f = 1$ , but again did not include the Uranian  $J_2/J_4$  terms, although the initial state vectors were adjusted in a simple manner to compensate for the lack of oblateness. The DL97(8J) model, referenced extensively in the current work, was also able to get close to  $m_f = 1$  and included the Uranian oblateness. However, these latter two models did not fully demonstrate the power law, since they did not actually verify the case of  $m_f = 1$ . With today's increasing computational capabilities, satellite systems with lower masses can be simulated all the way to orbit crossing. Nevertheless it is still true that the simulation time increases by approximately the fourth power of the reduction in mass for the Uranian system. This quickly results in an impractical simulation time for very low mass systems. As a result, the power law found by DL97 is still useful in many circumstances, and in this section we further explore its validity.

### 4.2. The validity of the power law

The simulations of the DL97(8J) model performed by DL97 covered a mass factor range of  $\sim 1.3$ –40. Smaller mass factors were not simulated due to the long simulation times required, and thus it was unproven whether the power law would continue to work at smaller mass factors. We started our exploration by reproducing their results. We ran a series of simulations with varying mass factors, in all cases represented by  $2^{n/10}$  for integer  $n$ . The initial orbital state vectors were not recomputed based on the new masses. For each simulation, we recorded the earliest time,  $t_c(m_f)$ , that any pair of satellites crossed orbits. We fit a power law using 50 data points over the

same mass factor range yielding  $\alpha = -4.3$  and  $\log \beta = 14.4$ . This is consistent with the power law fit using 46 data points found by DL97 of  $\alpha = -4.1 \pm 0.1$  and  $\log \beta = 14.1 \pm 0.1$ . Expanding the data to include mass factors of 0.933–1.231 and 40–64, we find a new power law fit that remains consistent with the fit found with the more restricted range of mass factors. In addition, the crossing time we found by direct integration,  $\log t_c(m_f=1) = 14.5$ , is consistent with the prediction of 14.3. Table 4 summarizes these results, which are shown graphically in Fig. 4.

Although the power law seems to work for chaotic systems in general, there is still the possibility that, below a particular mass assumption, the system ceases to be sufficiently chaotic that orbits would eventually cross. In this case, the power law would fail and yet we would have no indication of that in our current analyses. The first hint that this may be true was provided by the lowest mass factor simulation of the DL97(8J) model that we attempted ( $m_f = 0.871$ ), which was terminated before it found an orbit crossing. However, the lower bound provided by this simulation ( $1.330 \times 10^{15}$  sec) is well within the reasonable range of dispersions and thus does not prove that the model will never experience an orbit crossing.

To gain further insight into the situation, we can examine the progress of the orbits themselves. Fig. 5 shows the evolution of the apoapsis and periapsis of Cressida and Desdemona for  $m_f = 0.871$ , 0.933, and 1.000. In all three cases, the orbits appear chaotic for the first  $8 \times 10^{13}$  sec. With  $m_f = 1$  and 0.933, the orbits remain chaotic, leading relatively quickly to orbit crossings. However, with  $m_f = 0.871$ , the orbits become stable, experience a brief, unexplained interaction around  $5 \times 10^{14}$  sec, and then remain stable until  $\sim 1.05 \times 10^{15}$  sec, at which point they once again become chaotic. This qualitative difference in behavior from the  $m_f = 1$  and 0.933 cases may imply that the  $m_f = 0.871$  case is fundamentally different and will not lead to an orbit crossing. However, given the high variability of crossing times, it is also possible that the chaos will increase later and eventually cause an orbit crossing. Only a further exploration of mass factors in this area, with simulations run for much longer durations, will answer this question. Given the initial similarity of the three simulations considered here (Fig. 5, top), and the reappearance of chaos at  $5 \times 10^{14}$  sec and  $1.05 \times 10^{15}$  sec in the case of  $m_f = 0.871$  after long periods of stability, the short simulations used by Dawson et al. (2009, 2010) may not be capable of predicting long-term behavior.

#### 4.3. Multiple power laws

In both our models and the models of DL97, which pair of satellites crosses first is dependent upon the mass factor. For the I(*sat* $\pm$ ) models, Cupid and Belinda are usually the first pair to cross at low mass factors. However, at higher mass factors, Cressida, Desdemona, and Juliet become relatively more unstable and one of these adjacent pairs usually crosses first. This can be seen in Fig. 6 for the I(baseline) model, although a similar trend is present for the other models as well.

In their implementation of the power law, DL97 measured the time until the first pair of satellite orbits intersected, no matter which pair. Most often, it was Cressida and Desdemona, although occasionally it was Desdemona and Juliet. The challenge we have in applying the power law to our models is that we include Cupid, which we find to have a substantially shorter lifetime under most, but not all, circumstances. To account for this, we generalize the power law concept to one in which each pair of adjacent moons has a crossing time that can be modeled by a different power law. For simplicity, we assume that the distributions are Gaussians in  $\log t_c$  (as implied by Section 3.3), where each mean is defined by a power law with a different slope and

intercept. This view of the crossing events as a set of RVs with overlapping probability density functions also provides a natural framework within which we can understand a number of our anomalous integrations, such as the relatively rare cases where the first crossing involves Desdemona and Juliet or Rosalind and Cupid. Although the concept is valid for an arbitrary number of overlapping power laws, for practical reasons we will limit our analysis to two, representing Cressida–Desdemona and Cupid–Belinda. For simplicity, we remove any simulations that do not have Cupid–Belinda or Cressida–Desdemona cross first.

In a given integration, the first crossing time can be regarded as the minimum of two independent random variables (RVs), each describing the lifetime of a pair of satellites. Fig. 7 shows a Monte Carlo simulation of how the mean value of the minimum relates to the mean and standard deviation of the distributions. When the mean of one distribution is much smaller than that of the other, then our measurements are consistent with that distribution alone. However, if the means of the two RVs are comparable, then our crossing time becomes a distinctly biased measure of the expected crossing time for either RV alone; the measurements are low by about  $0.5 \sigma$  in the case where the means and standard deviations are equal.

The figure shows a distinct bend in observed value in this region, but in practice the scatter among our chaotic simulations can mask a relatively subtle bend. An alternative (and very intuitive) way to identify the rough location of the bend is the place where the most common first crossing transitions from one pair to the other. We can readily identify this situation in our integrations because we always know which pair of satellites crosses first. With a sufficient number of simulations at different mass factors, we can roughly determine the power laws of the satellite pairs independently.

Our process for determining the two sets of power law parameters ( $\alpha_{\text{cupid}}, \beta_{\text{cupid}}, \sigma_{\text{cupid}}, \alpha_{\text{cressida}}, \beta_{\text{cressida}}, \sigma_{\text{cressida}}$ ) begins by running a set of simulations with  $m_f = 2-64$  in steps of  $2^{n/10}$  for integer  $n$ . We also include a single simulation with  $m_f = 1$ , although the lengthy simulation times required for such small mass factors preclude us from running additional simulations with  $m_f < 2$ . We discard the results from any simulation where a pair of satellites other than Cressida–Desdemona or Cupid–Belinda crosses first. We next make a visual determination of the approximate mass factor where the crossing dominance switches from Cupid–Belinda to Cressida–Desdemona. The values chosen are shown in Table 5, but the exact value chosen does not have a strong effect on the end result. Given this value, which we will call  $m_{f,\text{intersect}}$ , we determine a series of eight metrics from our ensemble of simulations. These are, for the simulations with mass factors less than  $m_{f,\text{intersect}}$ : the fraction of simulations where Cupid–Belinda cross first, the slope and intercept of the best fit line to the Cupid–Belinda crossings, and the standard deviation of the Cupid–Belinda crossings about this line; for the simulations with mass factors greater than  $m_{f,\text{intersect}}$ , the metrics are repeated for Cressida–Desdemona crossings. Although many different metrics could be used, we find these metrics are sufficient to produce good results.

Given these metrics, we find a set of power law parameters that, when run through our Monte Carlo simulation, produces the same values for the metrics. We do this using a Nelder-Mead simplex algorithm to optimize the residuals found by computing the sum-of-squares of the differences between the eight metrics derived from the original orbital simulations and the eight metrics from the Monte Carlo simulations. We do not weight the metrics differently. To avoid problems with local minima, we run the optimization multiple times using different initial values of the power law parameters and then choose the result with the lowest final residual.

To determine error bars on the power law parameters, we perform the entire optimization procedure multiple times while perturbing the target metrics. Each time, the slope and intercept of the Cupid–Belinda crossings and the Cressida–Desdemona crossings are chosen from a normal distribution with a mean of the values computed from the original orbital simulations, and a standard deviation computed by the statistical goodness-of-fit of the lines to those simulations. The results for the 27 unit-density models are shown in Table 5, and plots of selected solutions are shown in Fig. 8. In all cases,  $\sigma_{\text{Cupid}}$  and  $\sigma_{\text{Cressida}}$  are approximately 0.3 and are not included in the table. Note that these uncertainties are similar to those derived from perturbing the initial state vectors (Section 3.3), increasing confidence in our methodology.

#### 4.4. Low satellite density

The densities of the inner Uranian satellites are unknown, but it is possible to set reasonable limits. Miranda, the innermost of the classical Uranian satellites, is relatively large (235 km radius) and has a density of  $1.2 \text{ g/cm}^3$  (Jacobson et al., 1992). This value, used by DL97 for all the inner satellites, is a conservative upper limit. However, the inner satellites are much smaller, more irregularly shaped, and are likely to be loose rubble piles. In this way they are more similar to the small icy satellites of Jupiter and Saturn than they are to Miranda. Amalthea, the largest of Jupiter’s inner moons, has a radius (83.5 km) similar to that of Portia and Puck and a density of  $0.857 \text{ g/cm}^3$  (Anderson et al., 2005). Saturn’s innermost satellites Pan, Atlas, Prometheus, Pandora, and Epimetheus, with sizes comparable to the smaller of the inner Uranian satellites, have densities ranging from 0.42 to  $0.64 \text{ g/cm}^3$ , with a general trend of increasing density with increasing size (Thomas, 2010). Finally, Neptune’s satellites Galatea and Despina may have densities of 0.4 to  $0.8 \text{ g/cm}^3$  (Zhang and Hamilton, 2008). As such, we choose  $0.5 \text{ g/cm}^3$  as a reasonable lower bound on the density of the inner Uranian satellites. As crossing time increases with decreasing mass, we will use this density to place an upper bound on crossing time.

Running multiple simulations at such a low density is possible, but requires substantial computation time. Instead, once the power law parameters have been found for a unit-density model, they can be used to extend the results to non-unit-densities (since our baseline model uses unit densities, a non-unit-density is equivalent to a mass factor). The resulting predicted crossing times for  $\rho = 0.5 \text{ g/cm}^3$  are shown in Table 5 and Fig. 9. Cupid and Belinda cross orbits on a timescale of  $1.0 \times 10^5$  to  $1.6 \times 10^7$  years and Cressida and Desdemona cross orbits on a timescale of  $1.3 \times 10^6$  to  $3.2 \times 10^7$  years, depending on the particular model used. In all cases, the time to first crossing is significantly less than the age of the solar system.

We now have a series of three masses for each satellite (radius decreased by one sigma, baseline, and radius increased by one sigma) and the corresponding crossing times for both Cupid–Belinda and Cressida–Desdemona for  $\rho = 0.5$ . By finding significant monotonic changes in crossing time with mass (defined here as changes whose  $1-\sigma$  uncertainties do not overlap), we can determine which satellites most affect the crossing times of these two pairs. It should be noted, however, that our one-sigma changes in radii are based on observational uncertainties, and thus the percentage mass change for each satellite is different. For example, the three mass models of Cressida only change mass by a total of 34%, while the three mass models of Belinda change mass by nearly a factor of three. Thus it is not appropriate to rank the level of influence of each satellite, only to note that such an influence exists.

Examining Fig. 9, we find that the stability of Cupid–Belinda increases with Cupid’s mass, but decreases with Belinda’s mass. We also find that Perdita has a strong influence, with

increasing mass decreasing stability. This is shown in Fig. 8, where the increase in the mass of Perdita, the third smallest satellite in the system, results in a pronounced bend in the power law.

Satellites far away from Cupid and Belinda have unexpected influence as well. Bianca appears to have a noticeable effect, with increasing mass resulting in decreased stability. Even more surprising, Mab appears to have an effect, with increasing mass resulting in increased stability. For the Cressida–Desdemona system, the relationships are less clear, perhaps due to the greater difficulty in fitting power law parameters to the secondary pair in our process, or perhaps due to the relatively small error bars on the masses of Cressida and Desdemona. Nevertheless, it appears that both Ophelia and Bianca have an effect on the stability, with increased mass resulting in greater stability.

## 5. LONG-TERM EVOLUTION

The power law allows us to explore the evolution of the system after the first orbit crossing, which happens on timescales that make direct integration impractical. To do this, we ran simulations with a modified set of satellites. In each case, two or more adjacent satellites were combined, using their initial state vectors, to simulate a perfectly inelastic collision. The semi-major axis of the new, combined satellite was derived from the sum of the orbital energies of the contributing satellites. The remaining orbital elements (eccentricity, inclination, argument of pericenter, longitude of the ascending node, and mean anomaly) were the mass-weighted mean of those from the contributing satellites. No new orbital fit was performed for the remaining, non-colliding satellites. It is important to realize that this methodology does not fully reproduce the state of the system at the time of the collision. In particular, it is likely that the orbits of other satellites will have evolved before the collision occurs, and those orbital changes are not being considered here. The likely end result is that the crossing times presented below are overestimates, since the non-colliding satellites will have had a chance to develop their chaotic interactions during the time required for other satellites to collide.

Although the chaos of the system makes it impossible to predict an exact cascade of collisions, we can nevertheless get an idea of what will happen by examining multiple simulations. To start this process, we examined the 250 position- and mass-perturbed simulations discussed in Section 3.3. 224 of these simulations had Cupid and Belinda cross orbits first, and thus we feel safe in using this assumption as the root of our cascade. Using these 224 simulations, Cupid and Belinda cross at a mean log time of 12.5 ( $\sim 1.0 \times 10^5$  years).

Performing new simulations with Cupid and Belinda combined into a single satellite, and taking advantage of the power law, yields a predicted log crossing time of 13.1 ( $\sim 4.0 \times 10^5$  years). In almost all of the simulations used to fit this power law, Cressida and Desdemona are the satellites that cross. We thus ran a new series of simulations with both Cupid and Belinda, and Cressida and Desdemona, combined. Because of the increased run times even at higher mass factors, we had to modify the range of mass factors used to 2.828–64. The power law yielded a predicted log crossing time of 15.2 ( $\sim 5.0 \times 10^7$  years). In almost all of these simulations, the combined Cressida–Desdemona satellite (colloquially named “Cresdemona”) collided with Juliet.

Continuing the process, the combined Cupid–Belinda satellite next collided with Perdita, with a projected log crossing time of 14.3 ( $\sim 6.3 \times 10^6$  years). Finally, after a combined time of  $\sim 57$  million years, we are left with a set of satellites where the two most unstable subsets

(Cressida–Desdemona–Juliet and Cupid–Belinda–Perdita) have been combined into single satellites. This system took substantially longer to experience crossing events, and we had to once again increase the starting mass factor to produce practical simulation times, this time to 32–512. The power law appears to still be valid in this range, yielding a predicted log crossing time of 22.0 ( $\sim 3.2 \times 10^{14}$  years). It is evident that at this point the system will remain stable for far longer than the predicted survival time of the solar system as a whole.

We can compare this cascade of collisions to the prediction of the Hill separations (Section 3.1). If we once again ignore the possible collision Juliet and Portia since empirically they are not as chaotic as predicted, the most favorable cascade is: Cupid and Belinda ( $\Delta = 10.12$ ), Cressida and Desdemona ( $\Delta = 11.78$ ), Cupid–Belinda and Perdita ( $\Delta = 18.38$ ), and Cressida–Desdemona and Juliet ( $\Delta = 21.06$ ). This sequence is similar to the empirical sequence above, with the exception that the Cupid–Belinda and Perdita and the Cressida–Desdemona and Juliet collisions are swapped. Thus the Hill separation criterion continues to be a good predictor of instability.

## 6. DISCUSSION

All 34 of the new models we investigated by direct integration showed instability and orbit crossing (and presumably eventual collisions), with time scales ranging from  $1.3 \times 10^3$  to  $1.6 \times 10^6$  years. Cupid and Belinda were usually the first satellites to cross orbits. Using the power law, we extended this result to densities of  $0.5 \text{ g/cm}^3$  and found that Cupid and Belinda crossed on time scales of  $1.0 \times 10^5$  to  $1.6 \times 10^7$  years while Cressida and Desdemona crossed on time scales of  $1.3 \times 10^6$  to  $3.2 \times 10^7$  years. Regardless of the particular mass and density assumptions used, it is probable that Cupid and Belinda will cross orbits within the next  $\sim 10$  million years, a small fraction of the total time since the formation of the Uranian system. Likewise, either before or after Cupid and Belinda collide, it is probable that Cressida and Desdemona will collide as well, and the apparent independence of the two groups of satellites implies that the order of collision is irrelevant. Thus the inner Uranian satellites are unstable on astronomically short timescales, and have likely already had multiple interactions since their formation.

While it is impossible to perform reverse integration on the system to determine the time of previous impacts, there is some evidence that such collisions have, in fact, occurred. Cupid is in a particularly precarious orbit and it is unlikely that we just happen to be observing it near the end of its lifespan. It is more likely that Cupid has been recently formed, perhaps as debris from a previous collision or as the accretion of dust produced by such a collision. Likewise, the  $\nu$  ring (Showalter and Lissauer, 2006), which exists between Portia and Rosalind, is located very close to Uranus' fluid Roche limit. As such, it may be in the process of accreting into a satellite.

The timescale of such an accretion is difficult to determine. Early works on disrupted satellites found that accretion would occur on a timescale of 10–100 years if tidal forces were ignored (Canup and Esposito, 1995). However, the  $\nu$  ring is well-entrenched in the Roche zone and tidal forces are important. Canup and Esposito (1995) found that, in this region, even perfectly inelastic collisions would only result in accretion under certain circumstances. In particular, the difference in the mass of the two colliding objects needs to be large, because otherwise each object will have significant portions existing outside of the Hill sphere of the other object and they will not become gravitationally bound. The mass difference requirement causes a bimodal distribution in the size of the resulting bodies as dust fails to aggregate with

other dust, but successfully combines with larger bodies. Such larger bodies have not been detected within the  $\nu$  ring, implying that either the  $\nu$  ring is relatively new, or that the largest bodies are still smaller than the current detection limit.

Another influence on the evolution of the satellites is the effect of meteoroid impacts and the associated catastrophic disruptions. Colwell et al. (2000) found that catastrophic disruptions of Cressida and Desdemona could occur every 0.9–6.2 Gyr, depending on assumptions about the internal strength of the satellites, while catastrophic disruptions of Belinda could occur every 1.3–9.1 Gyr. Such disruptions have likely already occurred at least once since the formation of the Uranian system. Thus, it is quite likely that even if Cressida and Desdemona, or Cupid and Belinda, were able to collide and accrete into a single new body, the resultant body would be broken apart by a subsequent meteoroid impact and the eventual stability of the inner Uranian satellites discussed in Section 5 will never come to pass.

In the end, there is little concrete we can say about the history or future of the inner Uranian satellites, except that we are undoubtedly not seeing them in their original configuration and what we see today will likewise evolve over astronomically short time periods. This evolution will be driven by orbital instabilities and resulting collisions, the dynamics of the accretion of the colliding bodies and any dusty rings produced from the collisions, and the random chance of catastrophic disruption by meteoroids.

### **Acknowledgments**

We thank the Centre for Astrophysics and Supercomputing at the Swinburne University of Technology, along with Professors Jarrod Hurley and Sarah Maddison, for access to the Swinburne “Green” supercomputer, which was used for many of the simulations in this paper. This work was performed under grant XXX.

## References

- Anderson, J.D., Johnson, T.V., Schubert, G., Asmar, S., Jacobson, R.A., Johnston, D., Lau, E.L., Lewis, G., Moore, W.B., Taylor, A., Thomas, P.C., Weinwurm, G. 2005. Amalthea's density is less than that of water. *Science* 308, 1291-1293.
- Borderies-Rappaport, N., Longaretti, P.-Y. 1994. Test particle motion around an oblate planet. *Icarus* 107, 129-141.
- Canup, R.M., Esposito, L.W. 1995. Accretion in the Roche zone: Coexistence of rings and ring moons. *Icarus* 113, 331-352.
- Chambers, J.E. 1999. A hybrid symplectic integrator that permits close encounters between massive bodies. *Mon. Not. R. Astron. Soc.* 304, 793-799.
- Chambers, J.E., Wetherill, G.W., Boss, A.P. 1996. The stability of multi-planet systems. *Icarus* 119, 261-268.
- Colwell, J.E., Esposito, L.W., Bundy, D. 2000. Fragmentation rates of small satellites in the outer solar system. *J. Geophys. Res.* 105, 17589-17600.
- Dawson, R.I., French, R.G., Showalter, M.R. 2009. Dynamical interactions among the small inner moons of Uranus. *Bull. Am. Astron. Soc.* 41, 899. DDA meeting abstract.
- Dawson, R.I., French, R.G., Showalter, M.R. 2011. Short-term interactions and chaos among the inner Uranian moons. *Icarus* submitted.
- Dawson, R.I., French, R.G., Showalter, M.R. 2010. Packed perturbers: Short-term interactions among Uranus' inner moons. *Bull. Am. Astron. Soc.* 41, 933. DDA meeting abstract.
- Duncan, M.J., Lissauer, J.J. 1997. Orbital stability of the Uranian satellite system. *Icarus* 125, 1-12.
- French, R.G., Nicholson, P.D., Porco, C.C., Marouf, E.A. 1991. Dynamics and structure of the Uranian rings. In: Bergstralh, J.T., Miner, E.D., and Matthews, M.S. (Eds.), *Uranus*. University of Arizona Press, Tucson, AZ, p. 327.
- Gladman, B. 1993. Dynamics of systems of two close planets. *Icarus* 106, 247-263.
- Jacobson, R.A. 1998. The Orbits of the inner Uranian satellites from Hubble Space Telescope and Voyager 2 observations. *Astron. J.* 115, 1195-1199.
- Jacobson, R.A., Campbell, J.K., Taylor, A.H., Synnott, S.P. 1992. The masses of Uranus and its major satellites from Voyager tracking data and earth-based Uranian satellite data. *Astron. J.* 103, 2068-2078.
- Karkoschka, E. 2001a. Voyager's eleventh discovery of a satellite of Uranus and photometry and the first size measurements of nine satellites. *Icarus* 151, 69-77.
- Karkoschka, E. 2001b. Comprehensive photometry of the rings and 16 satellites of Uranus with the Hubble Space Telescope. *Icarus* 151, 51-68.
- Levison, H.F., Duncan, M.J. 1994. The long-term dynamical behavior of short-period comets. *Icarus* 108, 18-36.
- Lissauer, J.J. 1995. Urey prize lecture: On the diversity of plausible planetary systems. *Icarus* 114, 217-236.
- Meyer, J.A., Lissauer, J.J. 2005. Dynamical instability and accretion in the closely-spaced inner Uranian moon system. *Bull. Am. Astron. Soc.* 37, 679. DPS meeting abstract.
- Mikkola, S., Innanen, K. 1995. Solar system chaos and the distribution of asteroid orbits. *Mon. Not. R. Astron. Soc.* 277, 497-501.
- Owen, W.M., Synnott, S.P. 1987. Orbits of the ten small satellites of Uranus. *Astron. J.* 93, 1268-1271.

- Powell, M.J.D. 1964. An efficient method for finding the minimum of a function of several variables without calculating derivatives. *The Computer Journal* 7, 155-162.
- Renner, S., Sicardy, B. 2006. Use of the geometric elements in numerical simulations. *Celest. Mech. Dyn. Astron.* 94, 237-248.
- Showalter, M.R., Dawson, R., French, R.G. 2010. Astrometry of the inner Uranian moons, and the trouble with Mab. *Bull. Am. Astron. Soc.* 41, 937. DDA meeting abstract.
- Showalter, M.R., Lissauer, J.J., French, R.G., Hamilton, D.P., Nicholson, P.D., de Pater, I., Dawson, R. 2008. HST observations of the Uranian outer ring-moon system. *Bull. Am. Astron. Soc.* 40, 431. DPS meeting abstract.
- Showalter, M.R., Lissauer, J.J. 2006. The second ring-moon system of Uranus: Discovery and dynamics. *Science* 311, 973-977.
- Smith, B.A., Soderblom, L.A., Beebe, R., Bliss, D., Brown, R.H., Collins, S.A., Boyce, J.M., Briggs, G.A., Brahic, A., Cuzzi, J.N., Morrison, D. 1986. Voyager 2 in the Uranian system - Imaging science results. *Science* 233, 43-64.
- Thomas, P.C. 2010. Sizes, shapes, and derived properties of the saturnian satellites after the Cassini nominal mission. *Icarus* 208, 395-401.
- Thomas, P., Weitz, C., Veverka, J. 1989. Small satellites of Uranus - Disk-integrated photometry and estimated radii. *Icarus* 81, 92-101.
- Wisdom, J., Holman, M. 1991. Symplectic maps for the n-body problem. *Astron. J.* 102, 1528-1538.
- Zhang, K., Hamilton, D.P. 2008. Orbital resonances in the inner neptunian system. II. Resonant history of Proteus, Larissa, Galatea, and Despina. *Icarus* 193, 267-282.

**Table 1**  
**Physical and orbital characteristics of Uranian satellites from DL97 model and this work.**

Satellite	DL97 $GM^a$ ( $\text{km}^3\text{s}^{-2}$ )	Radius (km)	$GM$ ( $\text{km}^3\text{s}^{-2}$ )	$GM (r-1 \sigma)$ ( $\text{km}^3\text{s}^{-2}$ )	$GM (r+1 \sigma)$ ( $\text{km}^3\text{s}^{-2}$ )
Cordelia		21±3 <sup>b</sup>	0.002589112466095 <sup>d</sup>	0.002589112466095	0.003864797617028
Ophelia		23±4 <sup>b</sup>	0.003401547497568 <sup>d</sup>	0.001917581514410	0.005502807544558
Bianca	0.003569068560288	27±2 <sup>b</sup>	0.005502807544558 <sup>d</sup>	0.004368306044999	0.006818471432415
Cressida	0.012051400333440	41±2 <sup>b</sup>	0.019268353339353 <sup>d</sup>	0.016583906962132	0.022227898158064
Desdemona	0.008169458879880	35±4 <sup>b</sup>	0.011986631787478 <sup>d</sup>	0.008328717144741	0.016583906962132
Juliet	0.024856013187720	53±4 <sup>b</sup>	0.041621779139926 <sup>d</sup>	0.032891317624839	0.041621779139926
Portia	0.055853605391520	70±4 <sup>b</sup>	0.095893054299822 <sup>d</sup>	0.080375712941637	0.113289116721840
Rosalind	0.008169458879880	36±6 <sup>b</sup>	0.013043691957471 <sup>d</sup>	0.007548432845759	0.020712899728762
Cupid		9±2 <sup>c</sup>	0.000203807686836 <sup>d</sup>	0.000095893054300	0.000372109782137
Belinda	0.013210188827040	45±8 <sup>b</sup>	0.025475960854435 <sup>d</sup>	0.014161139590230	0.041621779139926
Perdita		13±3 <sup>c</sup>	0.000614218776375 <sup>d</sup>	0.000279571586880	0.001145125219860
Puck	0.152960081155200	81±2 <sup>b</sup>	0.148575803703066 <sup>d</sup>	0.137839695623702	0.159855398947324
Mab		12±3 <sup>c</sup>	0.000483099702129 <sup>d</sup>	0.000203807686836	0.000943554105720
Miranda	4.399977849623880		4.403988880239192 <sup>e</sup>		
Ariel	90.29859336378001		86.48943821066345 <sup>e</sup>		
Umbriel	78.20084149059601		81.48337213859010 <sup>e</sup>		
Titania	235.2977975679480		228.6406014922988 <sup>e</sup>		
Oberon	201.1019491218120		190.9467780172403 <sup>e</sup>		

Sources: <sup>a</sup>DL97; <sup>b</sup>Karkoschka (2001); <sup>c</sup>Showalter and Lissauer (2006) with error bars as described in Section 2.2; <sup>d</sup>computed from the baseline radius at 1  $\text{g}/\text{cm}^3$  as described in Section 2.2; <sup>e</sup>SPICE kernel “ura083.bsp”.

**Table 2**  
**Description of models with crossing times and first satellites to cross.**

Model	Mass Version	$\log t_c$	Crossing Satellites
I(baseline/0.5)	Baseline ( $\rho = 0.5$ )	13.7	Cupid–Belinda
I(baseline/0.7)	Baseline ( $\rho = 0.7$ )	12.8	Cupid–Belinda
I(baseline)	Baseline ( $\rho = 1.0$ )	12.5	Cupid–Belinda
I(baseline/1.5)	Baseline ( $\rho = 1.5$ )	10.9	Cupid–Belinda
I(baseline/2.0)	Baseline ( $\rho = 2.0$ )	10.6	Cupid–Belinda
I(baseline/3.0)	Baseline ( $\rho = 3.0$ )	10.9	Cressida–Desdemona
I(Cordelia–)	Cordelia $r - 1\sigma_r$	12.2	Cupid–Belinda
I(Cordelia+)	Cordelia $r + 1\sigma_r$	12.4	Cupid–Belinda
I(Ophelia–)	Ophelia $r - 1\sigma_r$	12.6	Cupid–Belinda
I(Ophelia+)	Ophelia $r + 1\sigma_r$	12.9	Cupid–Belinda
I(Bianca–)	Bianca $r - 1\sigma_r$	12.9	Cupid–Belinda
I(Bianca+)	Bianca $r + 1\sigma_r$	12.3	Cupid–Belinda
I(Cressida–)	Cressida $r - 1\sigma_r$	12.5	Cupid–Belinda
I(Cressida+)	Cressida $r + 1\sigma_r$	13.0	Cupid–Belinda
I(Desdemona–)	Desdemona $r - 1\sigma_r$	13.0	Cupid–Belinda
I(Desdemona+)	Desdemona $r + 1\sigma_r$	12.3	Cupid–Belinda
I(Juliet–)	Juliet $r - 1\sigma_r$	12.5	Cupid–Belinda
I(Juliet+)	Juliet $r + 1\sigma_r$	13.1	Cressida–Desdemona
I(Portia–)	Portia $r - 1\sigma_r$	12.1	Cupid–Belinda
I(Portia+)	Portia $r + 1\sigma_r$	12.6	Cupid–Belinda
I(Rosalind–)	Rosalind $r - 1\sigma_r$	12.3	Cupid–Belinda
I(Rosalind+)	Rosalind $r + 1\sigma_r$	12.3	Cupid–Belinda
I(Cupid–)	Cupid $r - 1\sigma_r$	12.5	Cupid–Belinda
I(Cupid+)	Cupid $r + 1\sigma_r$	12.8	Cupid–Belinda
I(Belinda–)	Belinda $r - 1\sigma_r$	13.2	Cupid–Belinda
I(Belinda+)	Belinda $r + 1\sigma_r$	11.6	Cupid–Belinda
I(Perdita–)	Perdita $r - 1\sigma_r$	12.9	Cupid–Belinda
I(Perdita+)	Perdita $r + 1\sigma_r$	11.9	Cupid–Belinda
I(Puck–)	Puck $r - 1\sigma_r$	12.1	Cupid–Belinda
I(Puck+)	Puck $r + 1\sigma_r$	12.1	Cupid–Belinda
I(Mab–)	Mab $r - 1\sigma_r$	12.2	Cupid–Belinda
I(Mab+)	Mab $r + 1\sigma_r$	13.1	Cupid–Belinda
C(baseline)	Baseline ( $\rho = 1.0$ )	12.9	Cupid–Belinda
IO(baseline)	Baseline ( $\rho = 1.0$ )	13.1	Cupid–Belinda

**Table 3**  
**Orbit crossing time of the I(baseline) model with individual satellites removed.**

Satellite removed	$\log t_c$	Crossing Satellites
None	12.5	Cupid–Belinda
Cordelia	12.4	Cupid–Belinda
Ophelia	12.6	Cupid–Belinda
Bianca	11.9	Cupid–Belinda
Cressida	12.3	Cupid–Belinda
Desdemona	12.3	Cupid–Belinda
Juliet	12.1	Rosalind–Cupid
Portia	12.2	Cupid–Belinda
Rosalind	12.5	Cupid–Belinda
Cupid	13.5	Cressida–Desdemona
Belinda	13.7	Cressida–Desdemona
Perdita	13.7	Cressida–Desdemona
Puck	12.9	Rosalind–Cupid
Mab	12.1	Cupid–Belinda

**Table 4**  
**Power law parameters for the DL97(8J) model as published in DL97, reproduced in this work with the same mass factor range, and extended with a larger range of mass factors.**

Model	$m_f$ Range	# Data	$\alpha$	$\log \beta$
DL97(8J) (DL97)	~1.3–40	46	$-4.1 \pm 0.1$	$14.1 \pm 0.1$
DL97(8J) (This work)	1.3–40	50	$-4.3 \pm 0.0$	$14.4 \pm 0.1$
DL97(8J) (This work)	0.9330–64	62	$-4.1 \pm 0.0$	$14.3 \pm 0.1$

**Table 5****Dual power law Monte Carlo fits for Cupid–Belinda and Cressida–Desdemona with extrapolation to  $\rho = 0.5$  g/cm<sup>3</sup>.**

Model	$m_{f,intersect}$	$\alpha_{cupid}$	$\log \beta_{cupid}$	$\alpha_{cressida}$	$\log \beta_{cressida}$	$\log t_{c,cupid}$ ( $\rho = 0.5$ )	$\log t_{c,cressida}$ ( $\rho = 0.5$ )
I(baseline)	5.0	-3.1±0.3	12.5±0.2	-3.7±0.1	12.9±0.2	13.4±0.2	14.0±0.2
I(Cordelia–)	4.0	-2.5±0.3	12.2±0.1	-3.7±0.2	13.1±0.2	12.9±0.2	14.2±0.3
I(Cordelia+)	7.0	-2.8±0.3	12.4±0.1	-4.1±0.2	13.4±0.2	13.2±0.2	14.7±0.2
I(Ophelia–)	8.0	-3.2±0.2	12.5±0.2	-3.3±0.2	12.6±0.2	13.5±0.2	13.6±0.2
I(Ophelia+)	4.0	-3.4±0.5	12.7±0.2	-4.0±0.2	13.2±0.2	13.7±0.3	14.4±0.2
I(Bianca–)	8.0	-3.4±0.2	12.5±0.1	-3.7±0.2	12.8±0.2	13.6±0.2	13.9±0.2
I(Bianca+)	6.0	-2.6±0.3	12.1±0.2	-4.0±0.3	13.4±0.4	12.9±0.2	14.6±0.4
I(Cressida–)	5.0	-3.1±0.3	12.5±0.2	-4.2±0.2	13.6±0.2	13.5±0.3	14.8±0.2
I(Cressida+)	3.0	-3.5±1.1	13.0±0.4	-4.2±0.4	13.4±0.4	14.0±0.7	14.7±0.4
I(Desdemona–)	5.0	-3.3±0.5	12.9±0.2	-4.0±0.2	13.3±0.2	13.9±0.3	14.5±0.2
I(Desdemona+)	5.0	-2.8±0.5	12.4±0.3	-3.8±0.3	13.0±0.3	13.2±0.4	14.2±0.3
I(Juliet–)	9.0	-3.0±0.5	12.6±0.2	-3.8±0.4	13.4±0.4	13.5±0.3	14.6±0.4
I(Juliet+)	4.0	-3.6±0.6	12.9±0.3	-4.0±0.3	13.1±0.3	14.0±0.4	14.3±0.3
I(Portia–)	6.0	-2.5±0.4	12.1±0.3	-3.8±0.2	13.2±0.2	12.8±0.3	14.3±0.2
I(Portia+)	3.5	-2.9±0.9	12.3±0.3	-3.9±0.2	12.9±0.2	13.2±0.5	14.0±0.2
I(Rosalind–)	4.0	-2.4±0.5	12.3±0.2	-3.7±0.2	12.9±0.2	13.0±0.3	14.0±0.2
I(Rosalind+)	6.0	-3.0±0.3	12.4±0.2	-3.9±0.3	13.1±0.3	13.3±0.2	14.3±0.3
I(Cupid–)	4.0	-2.8±0.5	12.3±0.2	-3.9±0.1	13.1±0.2	13.1±0.3	14.3±0.2
I(Cupid+)	3.0	-3.7±0.3	12.9±0.1	-4.2±0.2	13.3±0.2	14.0±0.2	14.5±0.2
I(Belinda–)	3.5	-4.2±0.6	13.4±0.3	-4.5±0.3	13.6±0.3	14.7±0.4	15.0±0.3
I(Belinda+)	10.0	-2.9±0.3	12.1±0.2	-3.6±0.5	13.1±0.7	13.0±0.2	14.2±0.8
I(Perdita–)	3.0	-3.5±0.6	12.9±0.3	-4.1±0.2	13.4±0.4	13.9±0.4	14.6±0.4
I(Perdita+)	4.0	-2.0±0.4	11.9±0.2	-3.9±0.2	13.1±0.2	12.5±0.3	14.3±0.2
I(Puck–)	8.0	-2.6±0.3	12.3±0.2	-4.2±0.3	13.5±0.3	13.1±0.2	14.8±0.3
I(Puck+)	3.5	-2.8±0.6	12.2±0.2	-3.8±0.2	12.9±0.2	13.1±0.4	14.0±0.2
I(Mab–)	4.0	-2.9±0.4	12.3±0.2	-3.9±0.1	13.1±0.2	13.2±0.3	14.3±0.2
I(Mab+)	3.5	-3.6±0.4	12.8±0.2	-3.9±0.2	13.1±0.3	13.9±0.2	14.2±0.2

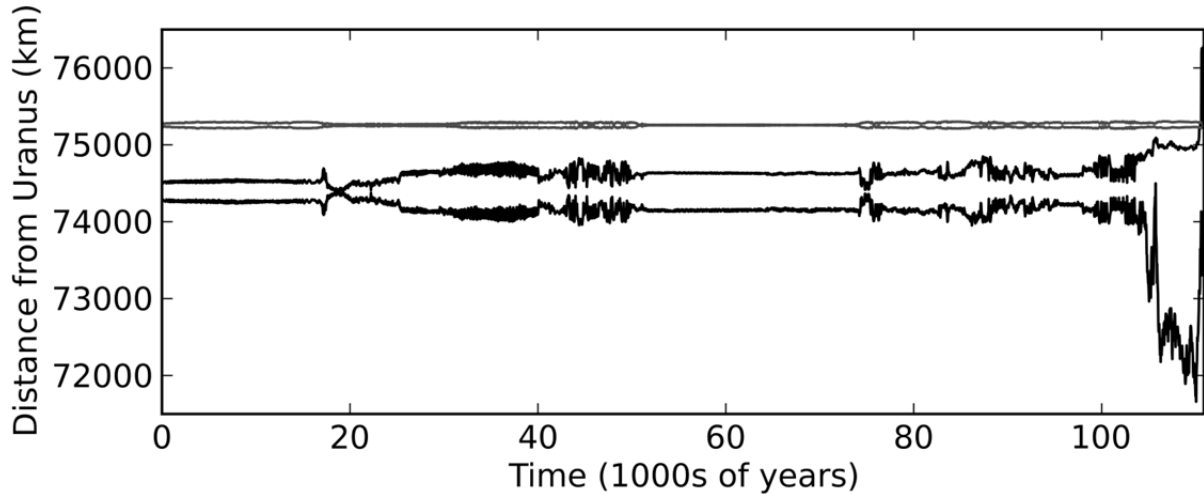


**Fig. 1:** The apoapsis and periapsis of Cupid (bottom, black) and Belinda (top, grey) until orbit crossing for the I(baseline) model.

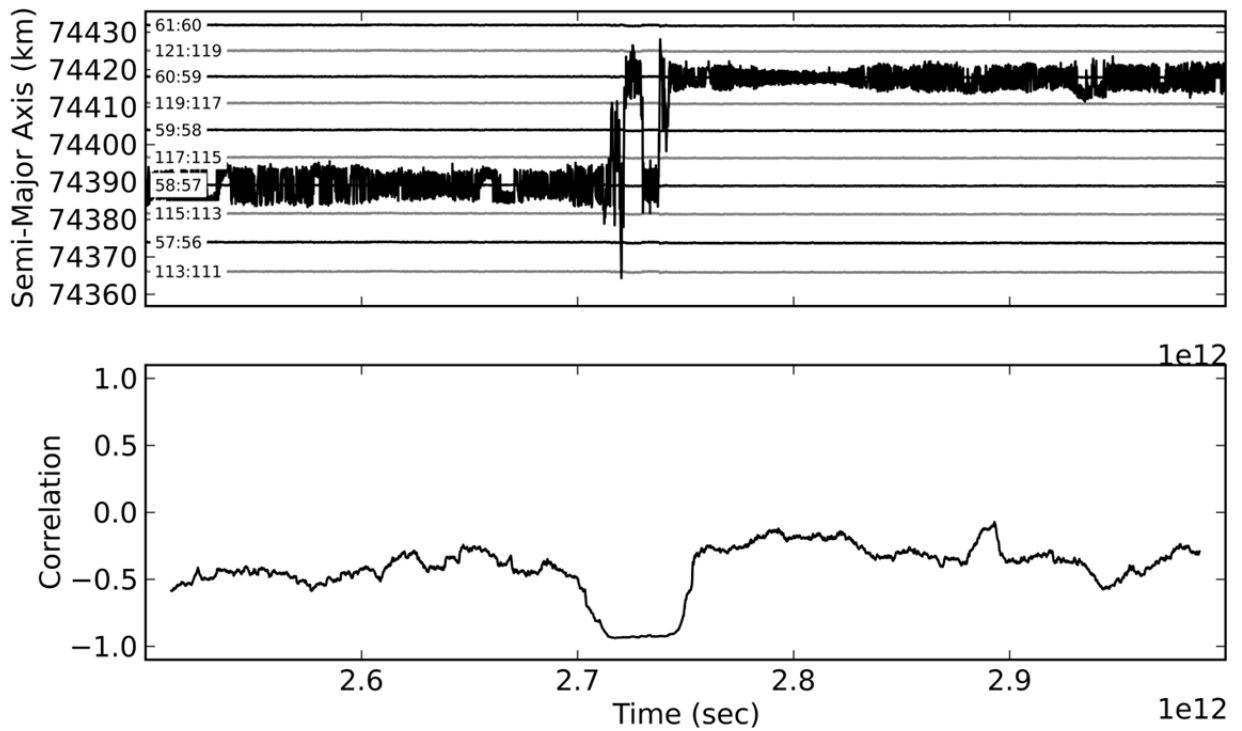


**Fig. 2:** The semi-major axis of Cupid overlaid on the first- and second-order inner Lindblad resonances of Belinda for the I(baseline) model (top). The correlation of the semi-major axis of Cupid with the semi-major axis of Belinda (bottom).

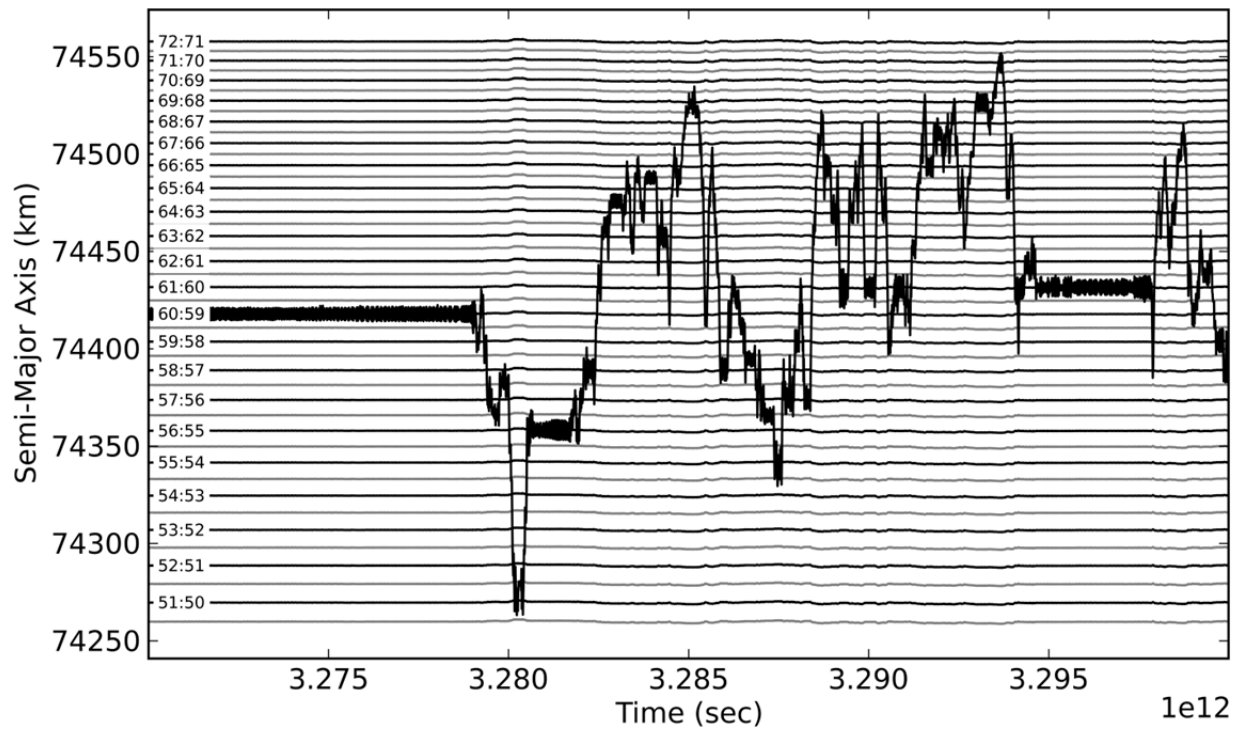


**Fig. 3:** The semi-major axis of Cupid overlaid on the first- and second-order inner Lindblad resonances of Belinda for the I(baseline) model. The simulation is shown starting at the time when Cupid becomes completely correlated with Belinda until the orbits eventually cross.

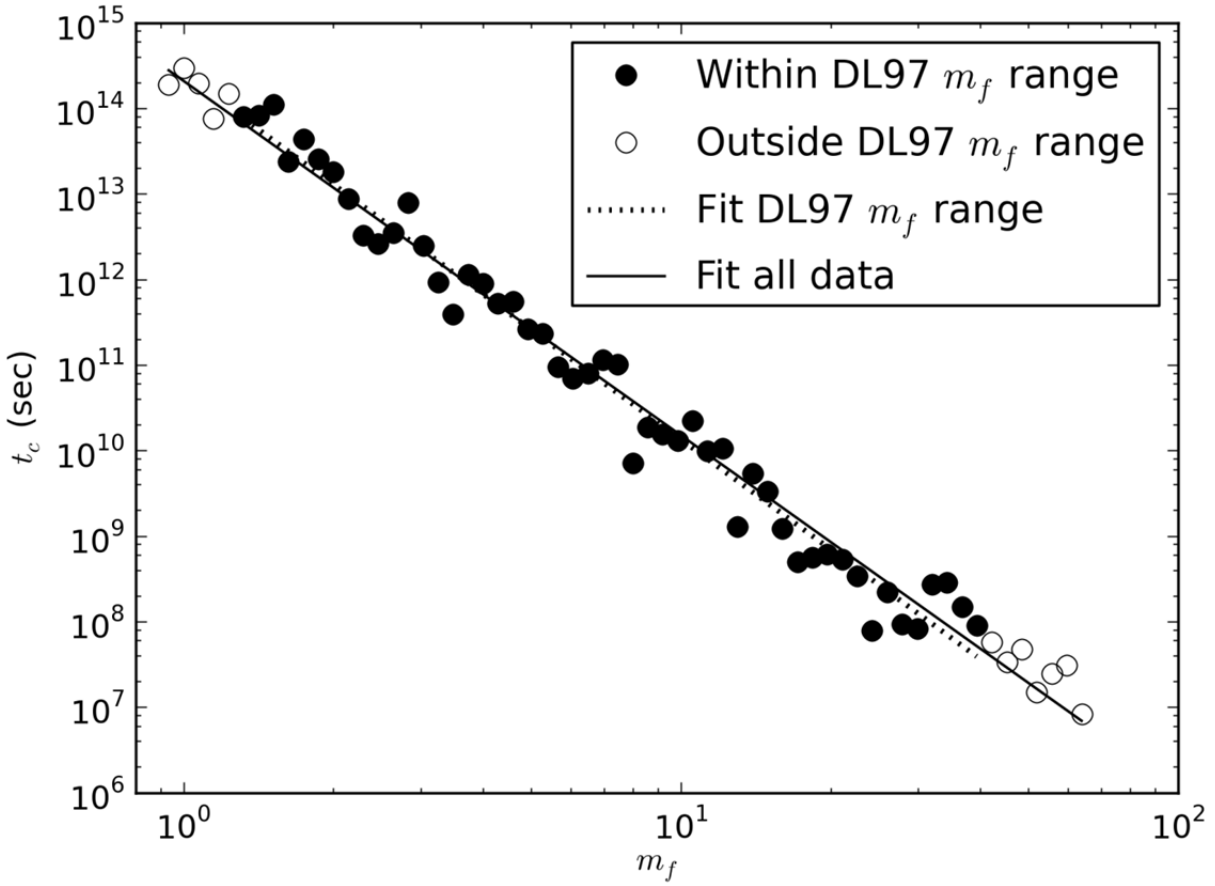


**Fig. 4:** Orbit crossing time vs. mass factor for the DL97(8J) model. The filled circles represent mass factors in the range of those covered in the original DL97 paper. The open circles represent mass factors that were added for this study. The dotted line is the power law fit to the filled circles and the solid line is the power law fit to all of the data shown.

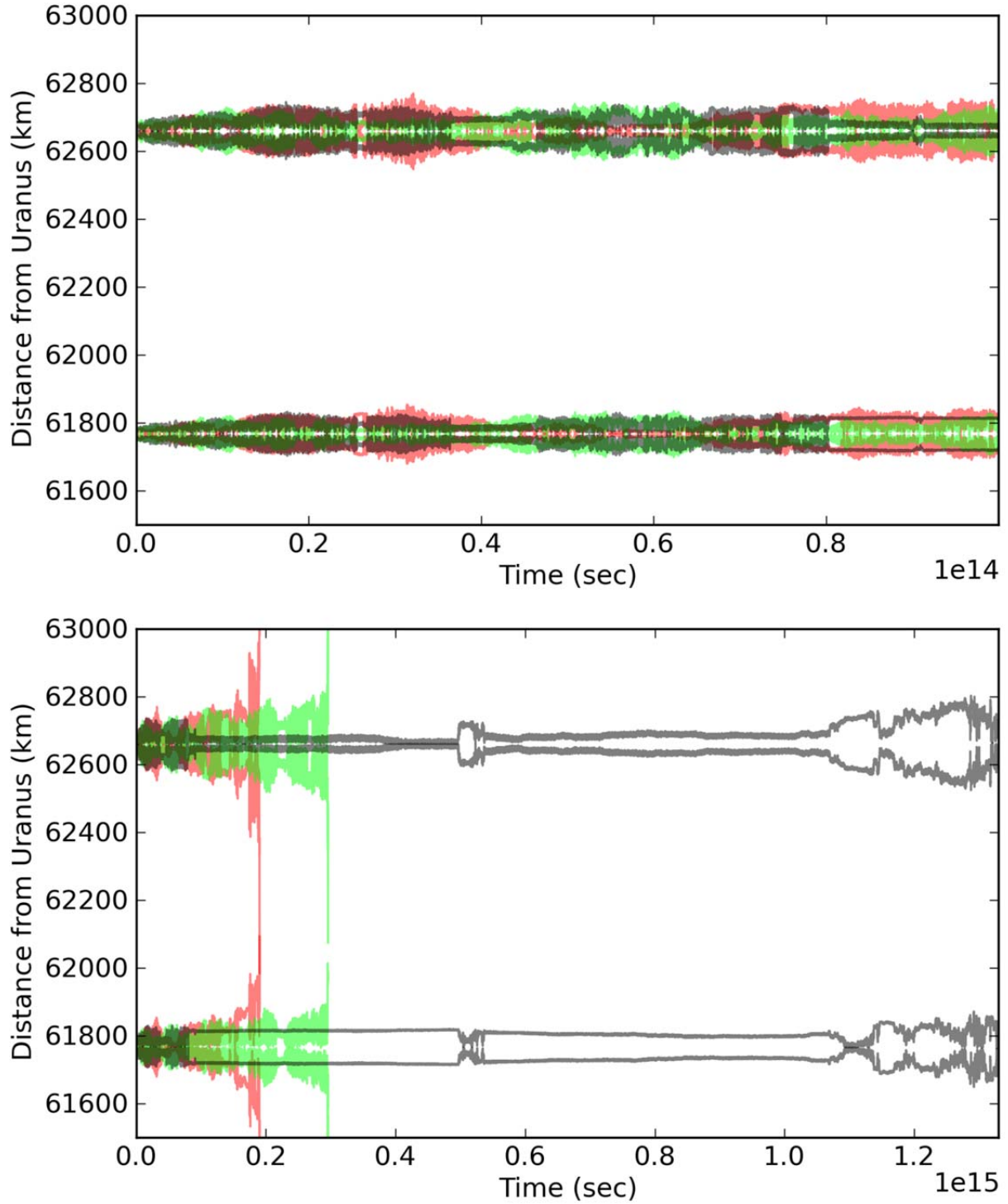
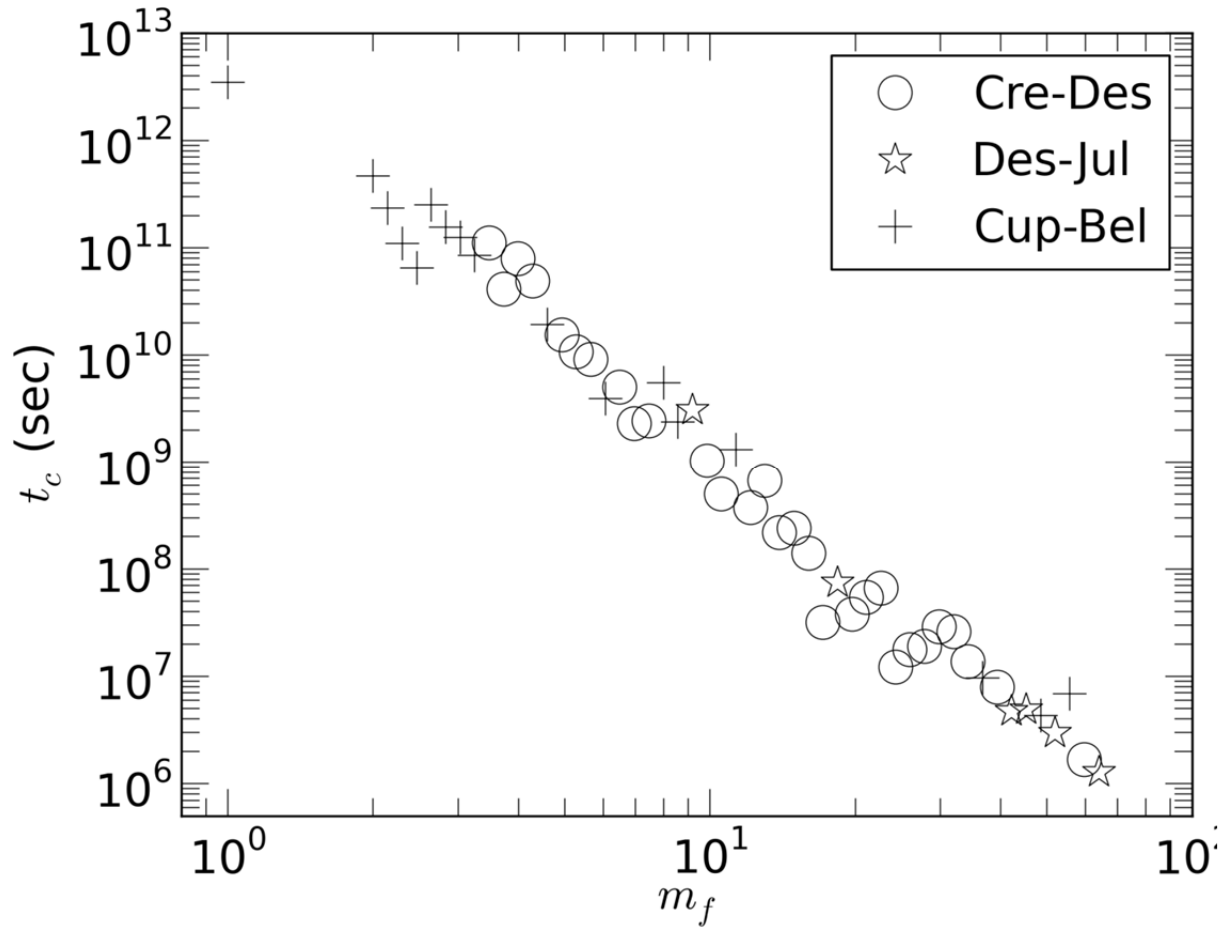


Fig. 5: Orbital progression of the periapsis and apoapsis of Cressida (bottom of each graph) and Desdemona (top of each graph) for the DL97(8J) model with  $m_f = 1$  (green),  $m_f = 0.933$  (red), and  $m_f = 0.871$  (black) for the first  $10^{14}$  sec (top) and for  $1.330 \times 10^{15}$  sec (bottom). The orbits for  $m_f = 1$  and  $m_f = 0.933$  are displayed until first orbit crossing.



**Fig. 6: Time of first crossing and which pair of satellites first crossed for various mass factors for the I(baseline) model.**

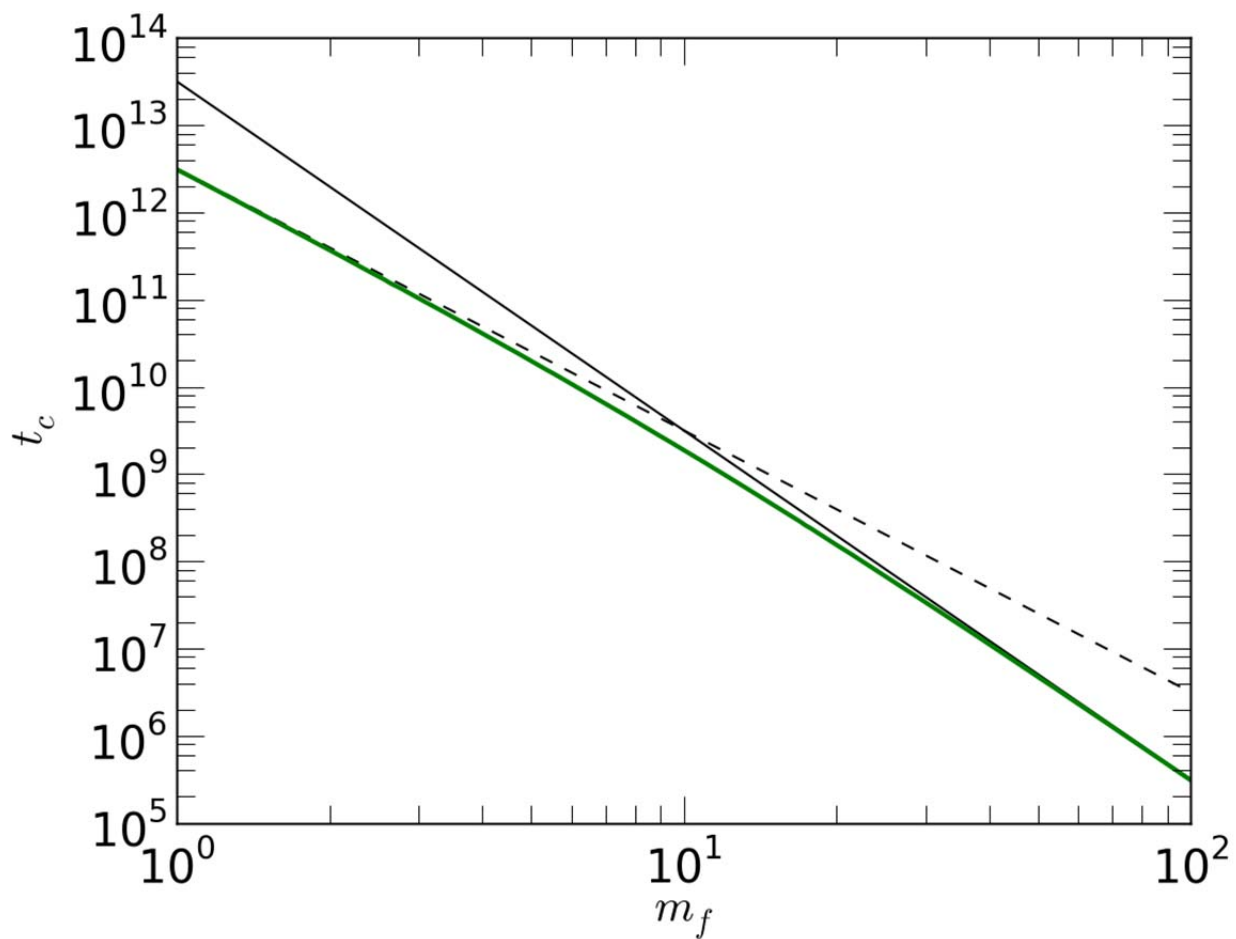


Fig. 7: Monte Carlo simulation showing the measured minimum time of crossing (green) vs. two power law modeled as random variables.

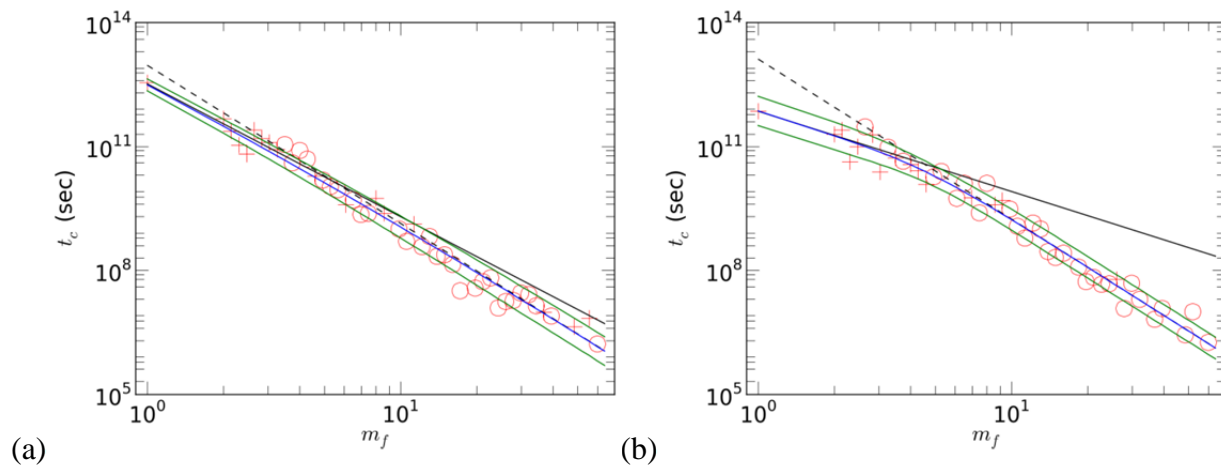


Fig. 8: Dual-power-law fits for the I(baseline) model (left) and I(Perdita+) model (right). Crosses indicate Cupid–Belinda crossings and circles indicate Cressida–Desdemona crossings.

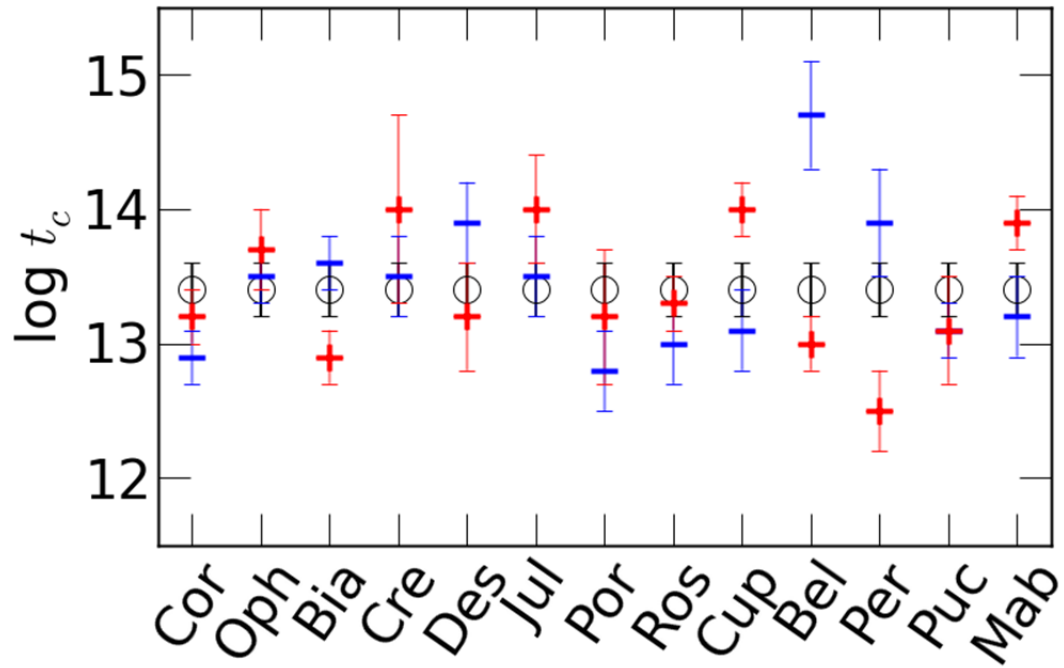


Fig. 9: Log crossing time for  $\rho = 0.5 \text{ g/cm}^3$  with the baseline mass assumptions (circles, black) and each satellite radius increased (+, red) or decreased (-, blue) by one sigma.